

RESEARCH ARTICLE

Open Access



Proteomic analysis of retinal pigment epithelium cells after exposure to UVA radiation

Jiunn-Liang Chen^{1,2,3}, Chun-Tzu Hung⁴, Joseph Jordan Keller^{5,6,7}, Hsien-Chung Lin^{4,8*†} and Yu-Jen Wu^{9*†}

Abstract

Background: Age-related macular degeneration (AMD) is the primary cause of blindness and severe vision loss in developed countries and is responsible for 8.7% of blindness globally. Ultraviolet radiation can induce DNA breakdown, produce reactive oxygen species, and has been implicated as a risk factor for AMD. This study investigated the effects of UVA radiation on Human retinal pigment epithelial cell (ARPE-19) growth and protein expression.

Methods: ARPE-19 cells were irradiated with a UVA lamp at different doses (5, 10, 20, 30 and 40 J/cm²) from 10 cm. Cell viability was determined by MTT assay. Visual inspection was first achieved with inverted light microscopy and then the DeadEnd™ Fluorometric TUNEL System was used to observe nuclear DNA fragmentation. Flow cytometry based-Annexin V-FITC/PI double-staining was used to further quantify cellular viability. Mitochondrial membrane potential was assessed with JC-1 staining. 2D electrophoresis maps of exposed cells were compared to nonexposed cells and gel images analyzed with PDQuest 2-D Analysis Software. Spots with greater than a 1.5-fold difference were selected for LC-MS/MS analysis and some confirmed by western blot. We further investigated whether caspase activation, apoptotic-related mitochondrial proteins, and regulators of ER stress sensors were involved in UVA-induced apoptosis.

Results: We detected 29 differentially expressed proteins (9 up-regulated and 20 down-regulated) in the exposed cells. Some of these proteins such as CALR, GRP78, NPM, Hsp27, PDI, ATP synthase subunit alpha, PRDX1, and GAPDH are associated with anti-proliferation, induction of apoptosis, and oxidative-stress protection. We also detected altered protein expression levels among caspases (caspase 3 and 9) and in the mitochondrial (cytosolic cytochrome C, AIF, Mcl-1, Bcl-2, Bcl-xl, Bax, Bad, and p-Bad) and ER stress-related (p-PERK, p-eIF2 α , ATF4 and CHOP) apoptotic pathways.

Conclusions: UVA irradiation suppressed the proliferation of ARPE-19 cells in a dose-dependent manner, caused quantitative losses in transmembrane potential ($\Delta\Psi_m$), and induced both early and late apoptosis.

Keywords: Proteomic, UVA, Retinal pigment epithelium cells, Apoptosis, Mitochondrial dysfunction

* Correspondence: m890070@gmail.com; wyr924@ms24.hinet.net; x00002180@meiho.edu.tw

[†]Hsien-Chung Lin and Yu-Jen Wu contributed equally to this work.

⁴Department of Ophthalmology, Yuan's General Hospital, Kaohsiung, Taiwan

⁹Department of Beauty Science, Meiho University, Pingtung, Taiwan

Full list of author information is available at the end of the article



Background

Age-related macular degeneration (AMD) is the primary cause of blindness and severe vision loss in developed countries and is responsible for 8.7% of blindness globally [1]. While the clinical progression of AMD is not well understood, the degeneration of retinal pigment epithelial (RPE) cells is suspected to be involved in the pathophysiology [2–5]. The exact cause of RPE cell degeneration is not clear. Numerous reports suggest that oxidative stress plays an important role in RPE apoptosis and the development of AMD [6–11], with current therapeutic strategies under investigation employing agents that reduce oxidative damage [12, 13]. Pathogenic mechanisms have been proposed to explain the complex etiology of AMD based on animal studies and cultured RPE cells, however, the molecular pathology is not yet entirely clear [14, 15].

Ultraviolet (UV) radiation is part of the electromagnetic spectrum. Only ultraviolet B (UVB; 280–320 nm) and ultraviolet A (UVA; 320–400 nm) reach the terrestrial surface [16]. Although the cornea, lens, and the vitreous body filter out most of the UV radiation below 400 nm, a portion of the UVA band (315–400 nm) penetrates the retina [17]. Ozone layer depletion, increased outdoor activity, and longer average life spans have contributed to the increased cumulative lifetime exposure of the retina to UV radiation [18]. UV irradiation can cause the production of reactive oxygen species (ROS), cellular changes, DNA damage, and apoptosis in RPE cells [19–24], and has been implicated as a risk factor for AMD. However, the results of studies investigating the association between UV exposure and AMD are inconsistent [19, 25–28].

In this study, comparative proteomic analysis was employed to identify the differential protein expression between ARPE-19 cells exposed to UVA radiation and unexposed control cells by comparing their 2D electrophoresis maps. These results will help clarify that UVA radiation induces damage to RPE cells at the molecular level, thus better elucidating the relationship between UVA radiation and AMD. This knowledge may benefit the development of preventive methods for UVA-induced retinal damage.

Methods

Reagents

Cell Extraction Buffer was produced by BioSource International (Camarillo, CA, USA). Dulbecco's modified Eagle's medium-F12 (DMEM-F12), fetal bovine serum (FBS) phosphate-buffered saline buffer (PBS), and trypsin-EDTA were manufactured by Biowest (Nuaille, France). The IPG buffer, protein assay kit 2-D Quant Kit, and IEF strips utilized in this study were produced by GE Healthcare (Buckinghamshire, UK). We used PVDF (polyvinylidenedifluoride) membranes that are

commercially available from Millipore (Bellerica, MA, USA). Sigma (St Louis, MO, USA) manufactured the protease inhibitor cocktail, dimethyl-sulfoxide (DMSO), 3-(4,5-Dimethylthiazol-2-yl)-2,5-diphenyltetrazolium bromide (MTT) and goat anti-rabbit or goat anti-mouse horseradish peroxidase conjugated IgG that were used in this study. Biotium (Hayward, CA, USA) and Pharmingen (San Diego, CA, USA) produced our cationic dye JC-1 (5,5,6,6-tetrachloro-1,1,3,3-tetraethylbenzimidazol-carbocyanine iodide) fluorescent kit and the Annexin V-FITC/PI Apoptosis Detection Kit, respectively. Promega (Madison, WI, USA) manufactured the 4'-6-diamidino-2-phenylindole (DAPI) and DeadEnd™ Fluorometric TUNEL fluorescent kits we used, and Pierce Biotechnology (Rockford, IL, USA) produced our ECL Western Blotting Reagent.

Cell culture

ARPE-19 (ATCC® CRL-2302™), a human retinal pigment epithelial cell line, was grown in DMEM-F12 medium supplemented with 10% (v/v) fetal bovine serum, streptomycin (100 µg/mL), and penicillin (100 units/mL) in a humidified atmosphere (5% CO₂ at 37 °C). We cultured ARPE-19 cells in 10 cm dishes. All the experiments were conducted in triplicate and then repeated three times to ensure reproducibility.

Determination of cellular viability following UVA irradiation

A UVA lamp (312 nm, Spectroline Model LF-106 M, EEC) was used as the UVA source. We first investigated the lethal UVA dose for the cells. A total of 1×10^5 cells were plated in 24-well plates and grown to 70% confluency. After removing the medium, the cells were rinsed twice with phosphate-buffered saline (PBS). The monolayer was then covered with 1 mL PBS and the cells irradiated with a UVA lamp at several doses (5, 10, 20, 30 and 40 J/cm²) from a distance of 10 cm. The original medium was replaced, and cellular viability was determined by MTT assay. Following a 24 h incubation, MTT solutions were added and the cells were incubated for an additional 3 h at 37 °C before removing the supernatant and adding 100 µL of DMSO. The absorbance was read at 560 nm with a microplate reader. A mock-irradiated control was also prepared using the same procedure without UVA irradiation. The morphological changes of the cells exposed to UVA radiation were observed with inverted light microscopy. To detect the cytotoxic effect of UVA irradiation on the induction of apoptosis, ARPE-19 cells were then exposed to 5 J/cm² and 10 J/cm² UVA radiation, incubated for 6 h, and stained with Annexin V-FITC/PI for flow cytometry analysis. Only the 5 and 10 J/cm² UVA irradiation dosages were used for the TUNEL/DAPI assay because

the of 20, 30 and 40 J/cm² UVA irradiation exposures resulted in severe cellular cytotoxicity and death.

4',6-diamidino-2-phenyl iodide (DAPI) and terminal deoxynucleotidyl transferase dUTP nick end labeling (TUNEL) stain

The staining procedure for DAPI/TUNEL has been described previously [29]. ARPE-19 cells (1×10^6 cells/well) were seeded in 12-well plates, irradiated with a UVA lamp at different doses (0, 5, and 10 J/cm²), and incubated for 24 h. We used DMSO as a control. The cells were all fixed with a 4% paraformaldehyde-PBS solution for 15 min and stained with DAPI prior to detecting nuclear DNA fragmentation with the DeadEnd™ Fluorometric TUNEL System (Promega, USA). Fluorescent microscopy was utilized to photograph the cells (Olympus IX71 CTS, Chinetek Scientific, Hong Kong, China).

Mitochondrial membrane potential ($\Delta\Psi_m$) assay using fluorescence microscopy

Mitochondrial membrane potential was assessed with 5, 5', 6, 6'-tetrachloro-1, 1', 3, 3'tetraethylbenzimidazolyl-carbocyanine iodide (JC-1) according to the manufacturer's protocol (Biotium, Hayward, CA, USA). ARPE-19 cells (1×10^5 cells/well) cultured in 12-well plates were exposed to UVA irradiation at different doses (control, 5, and 10 J/cm²) and grown in a 37 °C incubator for 24 h. Following incubation, we harvested the cells and washed them with PBS before adding 70 μ L of JC-1 staining solution and incubating them at 37 °C for 30 min in the dark [30]. The cells were directly observed with a fluorescent microscope (Olympus IX71 CTS, Chinetek Scientific, Hong Kong, China) after washing with PBS to remove unbound JC-1 dye.

2-DE analysis

The standard procedure for 2-DE was described in our previous study [31]. Three hundred micrograms of total protein was dissolved in rehydration buffer (8 M urea, 2% CHAPS, 40 mM DTT, 0.5% IPG buffer pH 3–10, and bromophenol blue) and loaded onto an IPG strip in a strip holder. We performed the first dimension electrophoresis at 20 °C on the IPGphor III (GE Healthcare). We rehydrated every 11-cm IPG strip (pI 3–10, Immobiline DryStrip) at 50 V for 12 h, before focusing as follows: 200 V (2 h), 500 V (2 h), 1000 V (2 h), 4000 V (2 h), 8000 V (4 h), until the total Vh reached 43,400 Vh. We then placed the equilibrated strip on a 12.5% SDS-PAGE gel for the second dimension electrophoresis. Visualization was achieved with CBR staining and images were analyzed with PDQuest 2-D Analysis Software (Bio-Rad, USA) for quantification. Spots with more than 1.5-fold difference were selected for further LC-MS/MS analysis.

Protein digestion and protein identification by LC-MS/MS

The standard procedure for protein identification by LC-MS/MS was described in our previous study [32]. Target protein spots were excised from the gel and allowed to undergo reduction by adding 100 μ L of 50 mM DTT/25 mM ammonium bicarbonate (pH 8.5) at 37 °C for 1 h. A further alkylating reaction was then performed through the addition of 100 μ L of 100 mM iodoacetamide/25 mM ammonium bicarbonate (pH 8.5) and reacted for 30 min in the dark at room temperature. We added 10 μ L of trypsin solution (10 ng/mL in 25 mM ammonium bicarbonate) to the gel, digested the protein for 24 h at 37 °C, and concentrated digestion peptide solution prior to LC-MS/MS analysis. We used an AB SCIEX QTRAP® 5500Q mass spectrometer (Applied Biosystems, CA, USA). The MS scan range was m/z 100 to 1000. Analyst 1.5.1 was used to process the raw data into a WIFF text file.

Western blot analysis

We purchased antibodies against Heat shock protein 27 (Hsp27), nucleophosmin (NPM), ATP synthase, and GAPDH from Epitomics (Burlingame, CA, USA) and antibodies against glucose-related protein 78 (GRP78), calreticulin (CALR), protein disulfide isomerase (PDI), cleaved-ATF6, ATF4, and PRDX1 antibodies were purchased from ProteinTech Group (Chicago, IL, USA). Antibodies against Bcl-xl, Mcl-1, Bcl-2, Bad, p-Bad, AIF, cytochrome C, PERK, p-PERK, eIF2 α , p-eIF2 α , CHOP, caspase-3, cleaved caspase-3, caspase-9, and cleaved caspase-9 were obtained from Cell Signaling Technology (Danvers, MA, USA). The protein collection and separation are explained elsewhere [33]. The primary antibody with appropriate dilution was incubated with the PVDF membrane at 4 °C for 2 h. The membrane was washed three times with PBST (10 mM NaH₂PO₄, 130 mM NaCl, 0.05% Tween 20), and then incubated with the second antibody (goat anti-rabbit or goat anti-mouse IgG and horseradish peroxidase conjugate, 1:5000 in blocking solution) at 4 °C for 2 h. The membrane was then washed three times with PBST. The western blot results were visualized through chemiluminescence by adding ECL Western Blotting Reagents (Pierce).

Statistical analysis

The results of the MTT assay were analyzed with Student's t-test (Sigma-Stat 2.0, San Rafael, CA, USA). Results with $p < 0.05$ were considered statistically significant.

Results

Cell viability after UVA irradiation

To examine the effect of UVA irradiation, ARPE-19 cells were exposed to various doses of UVA at 0, 5, 10, 20, 30 and 40 J/cm². Cellular viability was then determined by

MTT assay after a 24 h incubation. The results indicated that increasing doses of UVA radiation decreased ARPE-19 cell viability (Fig. 1a). The morphological changes of the cells exposed to UVA radiation were observed with inverted light microscopy. The growth of non-irradiated cells appeared compact and smooth; on the other hand, the cells treated with UVA irradiation above 10 J/cm² had decreased cell populations compared with their counterparts (Fig. 1b). The cell populations treated with 30 and 40 J/cm² UVA irradiation were reduced beyond the ability to appreciate them visibly, and thus are not presented.

UVA induced apoptosis of ARPE-19 cells

To detect the cytotoxic effect of UVA irradiation on the induction of apoptosis, ARPE-19 cells were exposed to 5 J/cm² and 10 J/cm² UVA radiation, incubated for 6 h, and then stained with Annexin V-FITC/PI for flow cytometry

analysis. An apoptotic rate of 3.1% was observed among the ARPE-19 cells following a 6 h 10 J/cm² UVA exposure, compared to the 0.11% apoptotic rate observed among the control sample (lower right quadrant of Fig. 2a). A late apoptotic cell rate of 5.55% was observed among the ARPE-19 exposed to 10 J/cm² of UVA, compared to the 0.44% apoptotic rate observed among the controls (Upper right quadrant of Fig. 2a).

These data demonstrate that UVA irradiation induced the apoptosis of ARPE-19 cells. To further validate the UVA-induced apoptosis of ARPE-19 cells, TUNEL/DAPI staining was performed to provide visual confirmation. UVA-induced massive apoptotic bodies were noted in ARPE-19 cells after exposure to 5 J/cm² and 10 J/cm² UVA radiation (Fig. 2b). These results clearly indicate that exposure to UVA radiation significantly induces the apoptosis of ARPE-19 cells, as determined by flow cytometric measurement and observation by fluorescence microscopy.

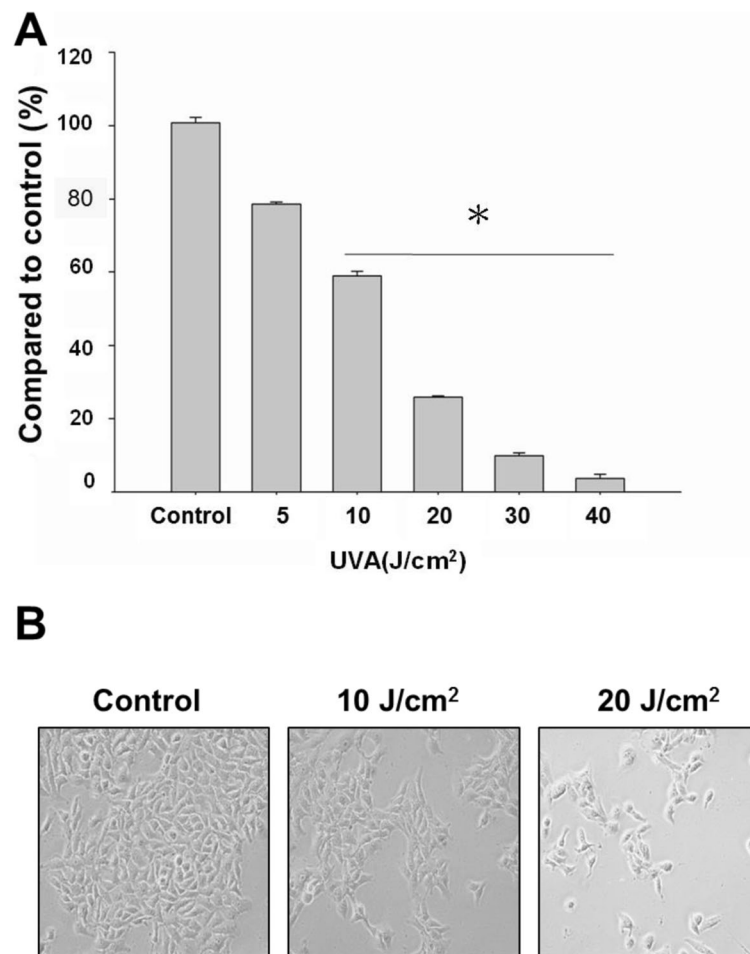


Fig. 1 Evaluation of UVA-irradiation on the cellular viability of ARPE-19 cells. **a** MTT assay demonstrated that the viable cell number of ARPE-19 cells was suppressed by UVA radiation. **b** Morphological changes of ARPE-19 cells following UVA exposure. The results shown are three independent experiments ([#] $p < 0.05$, * $p < 0.001$ compared with the control)

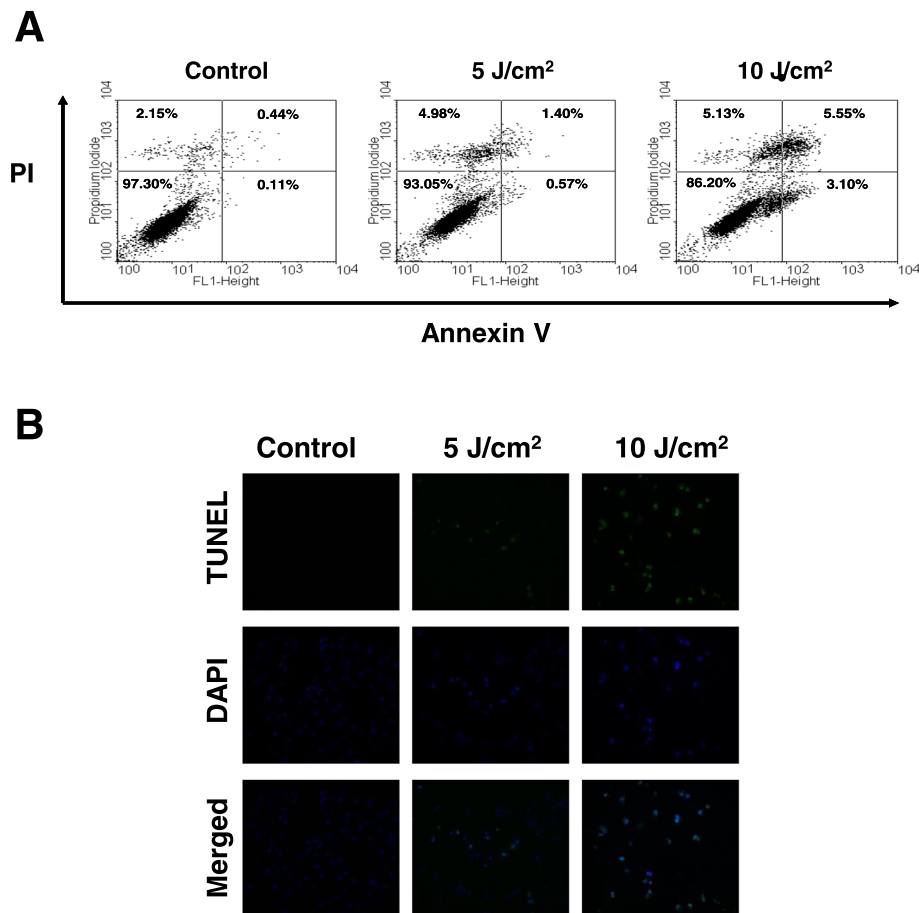


Fig. 2 UVA-induced apoptosis of ARPE-19 cells. **a** Detection of apoptotic ARPE-19 cells by Annexin V / PI analysis following UVA irradiation (0, 5 and 10 J/cm²). **b** Detection of apoptotic cells by TUNEL and DAPI staining following UVA irradiation (0, 5 and 10 J/cm²)

Proteomic analysis to identify changes in protein profile after UVA radiation of ARPE-19 cells

Both ARPE-19 cells exposed to 10 J/cm² UVA irradiation and unexposed cells were harvested. The proteins were extracted from cultured cells with cell extraction buffer. Following centrifugation, the supernatants were collected, and the proteins precipitated with 10% TCA/Acetone. The 2-DE maps of the non-irradiated ARPE-19 cells and 10 J/cm² UVA irradiated ARPE-19 cells were compared to examine the effect of UVA irradiation. A total of 300 μ g protein (*pI* 3–10) was loaded for the 2-DE experiments and visualized with CBR staining. PDQuest image analysis software (Bio-Rad) was employed to detect differential protein spotting (Fig. 3a).

Protein spots with more than a 1.5-fold difference were selected and further protein identification was performed using LC-MS/MS. Table 1 lists the identified proteins with their MASCOT scores, MS/MS matched sequences, apparent and theoretical *Mw/pI*, coverage, change in fold of expression level (up-regulation or down-regulation), cellular component, and protein function. Nine protein

spots were up-regulated and 20 protein spots were down-regulated following UVA exposure.

We classified these proteins into four groups according to their functions. The first group of proteins identified was involved in the stress response, cell proliferation, and apoptosis, including peroxiredoxin-1 (PRDX1), heat-shock protein 27 (Hsp27), protein disulfide-isomerase (PDI), calreticulin (CALR), 78 kDa glucose-regulated protein (GRP78), alpha crystalline B chain, cell division protein kinase 10, nucleophosmin (NPM), proteasome subunit alpha type-2, and regulator of G-protein signaling 21. The second group of proteins identified was related to glycolysis and energy metabolism, including triosephosphate isomerase, glyceraldehyde-3-phosphate dehydrogenase (GAPDH), L-lactate dehydrogenase A chain, fructose-bisphosphate aldolase A, and ATP synthase. The third group was related to cellular differentiation and the cytoskeleton, including tropomyosin alpha-4 chain, tubulin beta-4 chain, PDZ, and LIM domain protein 1. The fourth group was related to protein folding and other metabolism, including AH receptor-interacting protein (AIP), peptidyl-

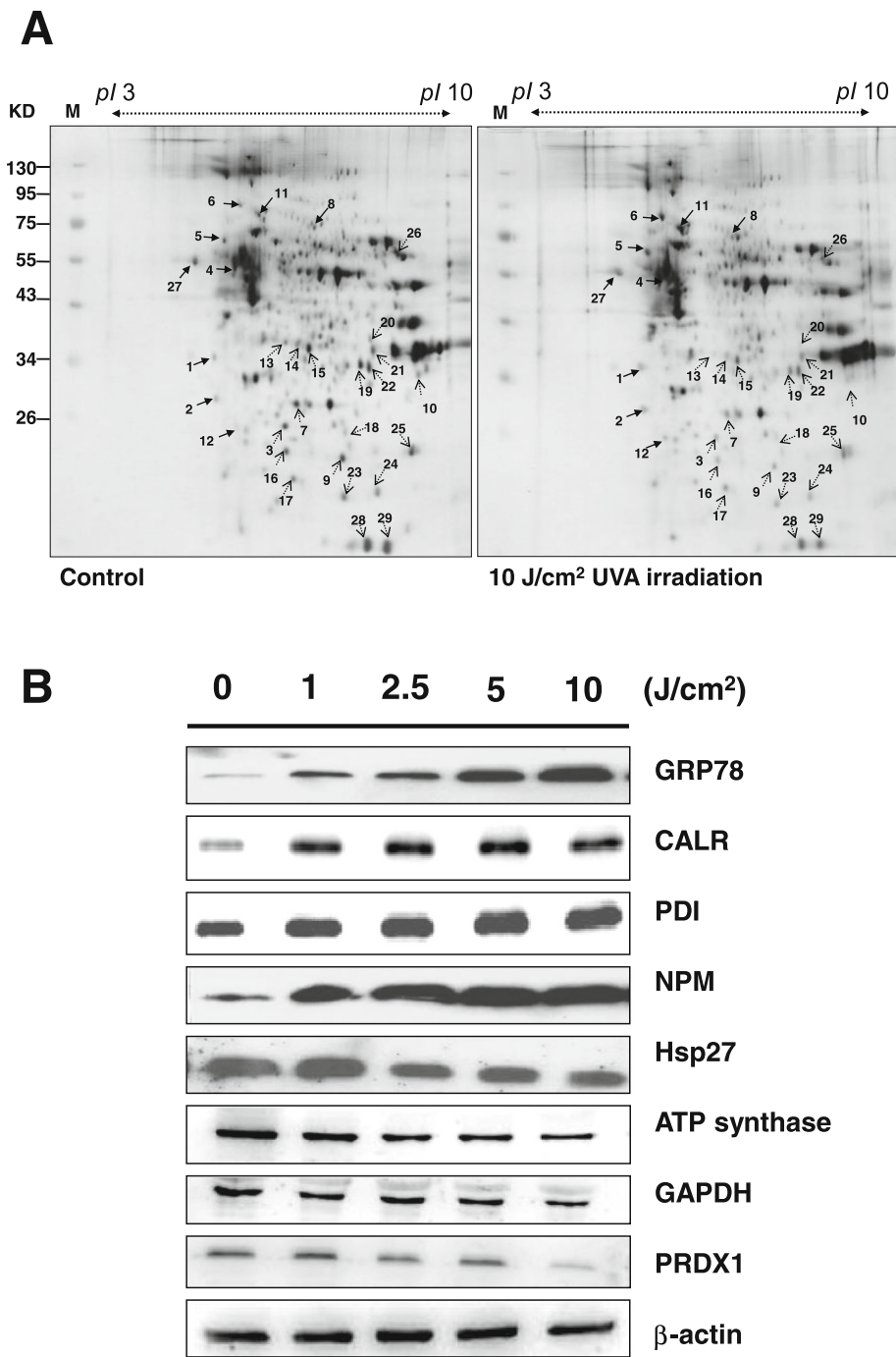


Fig. 3 Identification of the differentially expressed proteins between the control and UVA irradiated ARPE-19 cells by 2-DE. **a** ARPE-19 cells irradiated with 10 J/cm² UVA, followed by harvesting the cells and cell lysates. A total of 300 μg protein was then subjected to 2-DE and visualized by CBR staining. PDQuest image analysis software (Bio-Rad) was employed to explore differential expression through differential protein spotting. **b** Validation of identified selected proteins from 2-DE by western blot analysis. Some identified proteins include GRP78, CALR, PDI, NPM, Hsp27, ATP synthase, GAPDH, and PRDX1. β-actin was used as the loading control

prolyl cis-trans isomerase A, hydroxyacyl-coenzyme A dehydrogenase, and albumin.

To validate the differential expression pattern obtained from the 2-DE maps, several identified proteins were

investigated by western blotting using anti-CALR, GRP78, NPM, Hsp27, PDI, ATP synthase, PRDX1, and GAPDH specific antibodies. We observed four up-regulated proteins (CALR, GRP78, NPM, and PDI) and

Table 1 Proteins identification by LC/MS/MS

Pot no	Protein name	Accession.no	Calculate Mr/pl	Peptide matched	Sequence covered %	MASCOT score	Regulation (fold-change)	Cellular component	Protein function
1	Nucleophosmin	P06748	32.55/4.64	16	33	103	+ 2.64	Nucleus/ Cytoplasm	Cell proliferation/ apoptosis
2	Tropomyosin alpha-4 chain	P67936	28.5/4.67	4	18	61	+ 2.31	Cytoplasm	Cytoskeleton
3	Heat-shock protein 27	P04792	22.76/5.98	13	37	245	-1.92	Cytoplasm	Stress Response
4	Tubulin beta-4 chain	P04350	49.55/4.78	2	6	151	+ 2.72	Cytoplasm	Cytoskeleton
5	Protein disulfide-isomerase	P07237	57.08/4.76	7	15	89	+ 2.17	Endoplasmic Reticulum	Stress Response
6	78 kDa glucose-regulated protein	P11021	72.28/5.07	41	45	556	+ 4.19	Endoplasmic Reticulum	Stress Response
7	Triosephosphate isomerase	P60174	26.65/6.45	3	10	120	-2.08	Cytoplasm	Glycolysis
8	Bifunctional purine biosynthesis protein PURH	P31939	64.57/6.27	1	2	44	+ 2.64	Mitochondrion	Purine biosynthesis
9	Cell division protein kinase 10	Q15131	41.01/9.06	4	3	36	-3.08	Nucleus	Cell proliferation
10	L-lactate dehydrogenase A chain	P00338	36.66/8.44	12	23	145	-1.72	Cytoplasm	Glycolysis
11	Serum albumin precursor	P02768	69.32/5.92	31	11	194	+ 1.57	Cytoplasm	colloidal osmotic pressure of blood
12	Protein disulfide-isomerase A3	P30101	56.74/5.98	8	12	84	+ 2.72	Endoplasmic Reticulum	Stress Response
13	AH receptor-interacting protein (AIP)	O00170	37.64/6.09	2	6	49	-4.58	Cytoplasm	Protein folding
14	PDZ and LIM domain protein 1	O00151	36.04/6.56	4	13	59	-1.58	Cytoplasm	Cytoskeleton
15	PDZ and LIM domain protein 1	O00151	36.04/6.56	6	17	50	-1.56	Cytoplasm	Cytoskeleton
16	Heat-shock protein 27	P04792	22.76/5.98	83	59	874	-1.79	Cytoplasm	Stress Response
17	Heat-shock protein 27	P04792	22.76/5.98	25	31	121	-1.51	Cytoplasm	Stress Response
18	Proteasome subunit alpha type-2	P25787	25.99/6.92	16	38	111	-1.67	Nucleus/ Cytoplasm	Cell cycle/apoptosis
19	Putative GTP-binding protein 9	Q9NTK5	44.71/7.64	11	8	38	-1.51	Nucleus/ Cytoplasm	ATP catabolic process
20	Fructose-bisphosphate aldolase A	P04075	39.39/8.3	22	43	211	-1.71	Cytoplasm	Glycolysis
21	Glyceraldehyde-3-phosphate dehydrogenase	P04406	36.03/8.57	17	34	67	-1.92	Cytoplasm	Glycolysis
22	Hydroxyacyl-coenzyme A dehydrogenase	Q16836	34.25/8.88	16	19	69	-1.52	Mitochondrion	Fatty acid metabolism
23	Alpha crystallin B chain	P02511	20.14/6.76	57	47	524	-1.85	Cytoplasm	Stress Response
24	Regulator of G-protein signaling 21	Q2M5E4	17.66/6.59	2	12	45	-1.72	Cytoplasm	Signal transduction inhibitor
25	Peroxiredoxin-1	Q06830	22.32/8.27	23	46	273	-1.56	Cytoplasm	Stress Response
26	ATP synthase	P25705	59.71/9.16	13	13	65	-1.58	Mitochondrion	Energy metabolism
27	Calreticulin	P27797	48.28/4.29	133	71	3246	+ 1.69	Endoplasmic Reticulum	Stress Response
28	Peptidyl-prolyl cis-trans isomerase A	P62937	18.23/7.68	8	23	129	-1.62	Cytoplasm	Protein folding
29	Peptidyl-prolyl cis-trans isomerase A	P62937	18.23/7.68	45	60	1160	-1.72	Cytoplasm	Protein folding

four down-regulated proteins (Hsp27, PRDX1, ATP synthase, and GAPDH) in the UVA-irradiated ARPE-19 cells, which is consistent with the exhibited expression pattern from the 2-DE maps (Fig. 3b).

UVA irradiation induces the mitochondrial-related apoptotic pathway and caspase activation in ARPE-19 cells

UVA irradiation caused downregulation in the expression of ATP synthase, a mitochondrion-related protein involved in energy production. Mitochondria are essential to the intrinsic apoptotic pathway in which stressed cells engage in intracellular signaling that leads to the release of proteins from the mitochondrial intermembrane space. Mitochondrial dysfunction is therefore one characteristic of apoptosis and can be assessed through the change in mitochondrial transmembrane potential ($\Delta\Psi_m$). In the present study, we assessed the $\Delta\Psi_m$ with JC-1 dye and achieved visualization via fluorescent microscopy.

Staining with JC-1 permits for an assessment of mitochondrial health as it exhibits potential-dependent accumulation and indicates mitochondrial depolarization by a decrease in the red/green fluorescence intensity ratio. Red-fluorescent J-aggregates can be observed in healthy cells with high mitochondrial $\Delta\Psi_m$, while in apoptotic cells with low mitochondrial $\Delta\Psi_m$, the green-fluorescent monomeric form JC-1 is more apparent. The quantitative changes in transmembrane potential in this study were measured with a fluorescence plate reader to

detect the emission of red and green fluorescence. In the present study, we assessed the color and pattern of JC-1 fluorescent staining to evaluate mitochondrial function following exposure of ARPE-19 cells to UVA radiation. We observed a markedly increased green fluorescence and reduction in red fluorescence following UVA irradiation (Fig. 4a). These results suggest that UVA irradiation led to a loss of $\Delta\Psi_m$ and increased mitochondrial dysfunction.

To verify whether the mitochondrial-related apoptotic pathway is involved in UVA-induced apoptosis, we further detected several apoptotic-related mitochondrial proteins, including cytosolic cytochrome C, AIF, Mcl-1, Bcl-2, Bcl-xl, Bax, Bad, and p-Bad. The protein expression levels of cytosolic cytochrome C, AIF, Bax, and Bad were significantly increased in ARPE-19 cells following UVA irradiation. On the contrary, the protein expression levels of Mcl-1, Bcl-2, Bcl-xl, and p-Bad were significantly decreased following UVA exposure (Fig. 4b).

Caspase-3 and caspase-9 are known to be involved in cell apoptosis. We further investigated whether caspase activation was involved in UVA-induced apoptosis. In Fig. 4b, the western blotting results demonstrate that the expression levels of inactive pro-caspase-3 and pro-caspase-9 were decreased in the UVA-irradiated ARPE-19 cells while the expression levels of cleaved caspase-3, resembling active 17 kDa proteolytic fragments, and cleaved caspase-9, resembling active proteolytic 37 kDa fragments, were increased following UVA-irradiation.

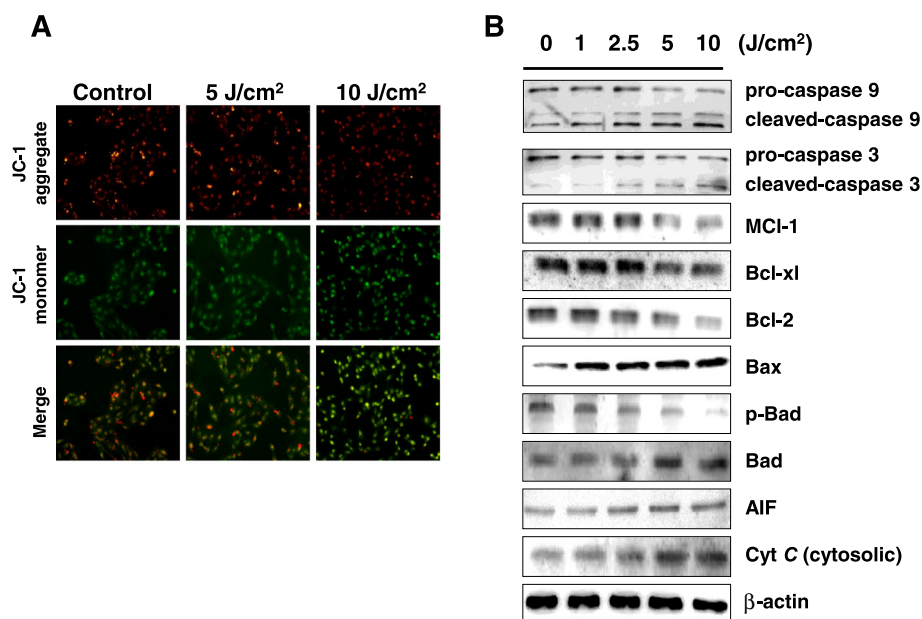


Fig. 4 UVA-irradiation led to loss of mitochondrial membrane potential and induced mitochondria-related apoptotic pathways in the AREP-19 cells. **a** Cells were exposed to UVA (0, 5 and 10 J/cm²), stained with JC-1 dye, and imaged under fluorescent microscopy. **b** Western blotting data showed changes in pro-caspase-3, cleaved-caspase-3, pro-caspase-9, cleaved-caspase-9, Mcl-1, Bcl-xl, Bcl-2, Bax, Bad, p-Bad, AIF, and cytosolic cytochrome C expression in AREP-19 cells exposed to UVA. β -actin was used as an internal control

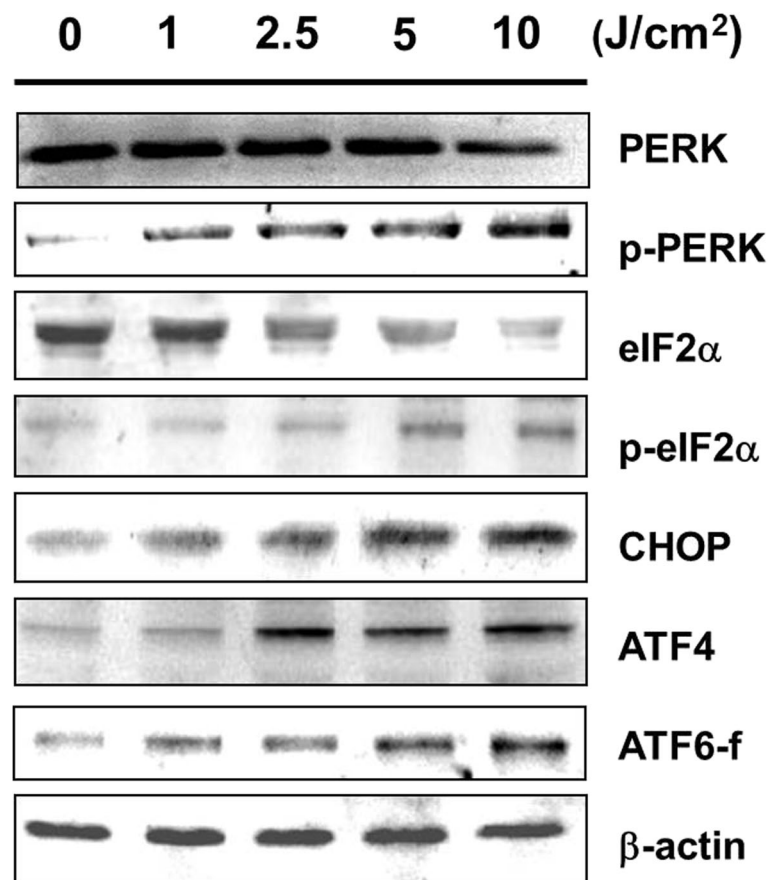


Fig. 5 UVA-irradiation stimulated factors of the ER stress-mediated apoptotic pathway. The changes in ER stress sensors PERK, p-PERK, e-IF2, p-eIF2, ATF4, CHOP, and ATF6 fragment were investigated by western blot analysis. β -actin was used as the internal control

UVA radiation induces the ER stress-related pathway in APRE-19 cells

We used western blot to verify regulators of ER stress sensors, including PERK, ATF6, GRP78, PDI, and CALR. The expression of ER chaperones GRP78, PDI, and CALR following UVA-irradiation were up-regulated in a dose dependent fashion (Fig. 3b). Up-regulation was also noted for p-PERK and p-eIF2 (Fig. 5). A downstream signal of the PERK-eIF2 pathway, ATF4, was also upregulated following UVA-irradiation of APRE-19 cells, as was CHOP, an ER stress-induced nuclear protein (Fig. 5).

Discussion

AMD is a leading cause of severe visual loss and blindness among the elderly population of the developed world [34]. The impairment of RPE cell function and degeneration of RPE cells are early and crucial events in the molecular pathology of AMD [2–5]. Oxidative damage is thought to play a critical role in the pathogenesis of AMD [8–11], and treatment with antioxidants has been demonstrated to reduce the progression of the pathology [13]. Overexposure to UV

radiation, which is released by the sun and by other artificial sources such as tanning beds and sun lamps, causes the production of reactive oxygen species (ROS) that may cause oxidative damage to RPE cells [11] and contribute to the onset of AMD [28].

Our study investigated the cytotoxic effect of UVA radiation on ARPE-19 cell as examined by MTT assay, flow cytometry, fluorescent staining assays, proteomic analysis, and western blot analysis. As expected, ARPE-19 cells underwent cell apoptosis following UVA exposure. Flow cytometric analysis demonstrated that UVA radiation induces both early and late apoptosis. We also used comparative proteomic analyses to detect changes in the protein expression profiles of ARPE-19 cells exposed to UVA light. Some of these proteins such as CALR, GRP78, NPM, Hsp27, PDI, ATP synthase subunit alpha, PRDX1, and GAPDH are anti-proliferative, induce apoptosis, and provide protection against oxidative-stress.

We used several validation methods to prove that UVA irradiation induced apoptosis. We used TUNEL/DAPI staining to detect apoptotic signaling cascades as well as confirm UVA-induced apoptosis of ARPE-19 cells (Fig. 2).

Change in mitochondrial transmembrane potential ($\Delta\Psi_m$) is a critical coordination event of apoptosis. Mitochondrial $\Delta\Psi_m$ change-induced pro-apoptotic events include the release of cytochrome C, which activates caspase-9 and in turn caspase-3, and the suppression of Bcl-2, Mcl-1, and Bcl-x1 expression [35]. In our study, JC-1 staining revealed that UVA exposure led to a loss of mitochondrial $\Delta\Psi_m$. Following UVA exposure, western blot analysis revealed that the ARPE-19 cells had increased expression of pro-apoptotic proteins such as cytosolic cytochrome C, cleaved-caspase-3, cleaved-caspase-9, Bad and Bax, and decreased expression of anti-apoptotic factors Mcl-1, Bcl-2, Bcl-x1, and p-Bad. These results indicate the caspase-3, caspase-9, and mitochondria-mediated apoptotic pathways were involved in the UVA-induced apoptosis of ARPE-19 cells.

In the present study, 2-DE and western blot analyses indicated that the expression levels of ER chaperones GRP78, PDI, and CALR were increased after UVA-irradiation. Moreover, the expression levels of GRP78, CALR, and PDI increased in a dose-dependent manner with UVA exposure (Fig. 3b). The altered protein expression levels of GRP78, PDI, and CALR also suggest that the ER stress-induced apoptotic pathway was activated upon UVA-irradiation of ARPE-19 cells.

The accumulation of unfolded proteins in the ER causes the release of transmembrane ER proteins involved in inducing the unfolding protein response. In normal cells, GRP78 binds to transmembrane ER signaling proteins like PERK, IRE1 α , and ATF6 [36–38] and activates them upon accumulation of unfolded proteins. PERK phosphorylates eukaryotic initiation factor 2 (eIF2 α) to promote translation of activating transcription factor 4 (ATF4) and pro-apoptotic transcription factor CHOP [39]. However, up-regulation of GRP78 can help prevent cell death due to ER stress [40] through the inhibition of cytochrome C-mediated caspase activation [41].

We also analyzed the PERK-eIF2 α -ATF4-CHOP signal pathway and another UPR sensor ATF6 to confirm the role of ER stress in UVA-induced apoptosis. The expression of p-RERK, p-eIF2 α , ATF4, CHOP, and ATF6-f expanded significantly following UVA-irradiation (Fig. 5), suggesting the involvement of the PERK-eIF2 α -ATF4-CHOP signal pathway and ATF6 due to the ER stress induced by UVA irradiation. In addition to confirming the role of ER stress in UVA-induced ARPE-19 apoptosis, these results may also suggest that GRP78 serves as a therapeutic target in AMD.

We also used comparative proteomic analyses to detect changes in the protein expression profiles of ARPE-19 cells exposed to UVA light. LC-MS/MS analysis identified 29 differentially expressed proteins (9 up-regulated and 20 down-regulated) in the ARPE-19 cells exposed to 10 J/cm² of UVA light. These proteins were classified into four groups: (1)

stress response, cell proliferation, and apoptosis; (2) energy metabolism; (3) cell differentiation and cytoskeleton; (4) protein folding and other metabolism. The change in expression of these proteins was verified by western blot.

The first group of proteins identified was involved in the stress response, cell proliferation, and apoptosis, including peroxiredoxin-1 (PRDX1), heat-shock protein 27 (Hsp27), protein disulfide-isomerase (PDI), calreticulin (CALR), 78 kDa glucose-regulated protein (GRP78), alpha crystalline B chain, cell division protein kinase 10, nucleophosmin (NPM), proteasome subunit alpha type-2, and regulator of G-protein signaling 21. In a prior study investigating proteome changes in a rat model of UV-induced AMD, Kraljević Pavelić et al. also observed the involvement of crystallins [42]. They specifically detected the involvement of Gamma-crystallin D, which when irradiated leads to structurally specific modifications and precipitation via side chain damage, polypeptide crosslinking, or fragmentation by way of amorphous aggregates and amyloid fibers [43]. Crystallins also have aromatic residues which undergo thermal and photochemical reactions when exposed to UV light. These reactions have been suggested to impair the folding and stability of crystallin and contribute to cataractogenesis [44]. The alpha crystalline investigated in the present study is a particularly important structural protein of the lens [45, 46] and has been suggested to play a protective role against oxidative stress and retinal degeneration [47].

The second group of proteins identified was related to glycolysis and energy metabolism, and included triose-phosphate isomerase, glyceraldehyde-3-phosphate dehydrogenase (GAPDH), L-lactate dehydrogenase A chain, fructose-bisphosphate aldolase A, and ATP synthase. Kraljević Pavelić et al. also observed that UV-radiation caused severe disruption of retinal metabolism, reducing metabolic activity and deregulating energy homeostasis, and detected a down-regulation of glycolytic enzymes, ATP production, and the citric acid cycle [42]. The retina has highest metabolic rate of all the tissues in the body [48] and over 50% of its ATP is derived through glycolysis [49]. Thus, our findings indicating UVA irradiation's effect on the expression of glycolytic proteins may help support the notion that UV irradiation can proceed through hampering retinal cells' ability to produce energy to cause the photoreceptor dysfunction and death characteristic of AMD.

The third group of differentially expressed proteins was related to cellular differentiation and the cytoskeleton, and included tropomyosin alpha-4 chain, tubulin beta-4 chain, PDZ, and LIM domain protein 1. The cytoskeleton plays an important role in vision. Some of its many and diverse functions include active transport, photoreceptor maintenance, and protein trafficking [50].

Narimatsu et al. demonstrated that light exposure works through oxidative stress to disrupt the actin cytoskeleton of RPE in mice [51]. Kraljević Pavelić et al. showed that in the rat retina UVB exposure proceeds through the activation of Src kinase to remodel and disintegrate the cytoskeleton [42], and Cachafeiro et al. suggested that photoreceptor cell death in AMD is caused by the light exposure-induced activation of Src kinase in the eye-cup and neural retina [52].

The fourth group of differentially expressed proteins observed in this study was related to protein folding and other metabolism, including AH receptor-interacting protein (AIP), peptidyl-prolyl cis-trans isomerase A, hydroxyacyl-coenzyme A dehydrogenase, and albumin. Kraljević Pavelić et al. also noted greater levels of serum albumin in rat retinas exposed to UV radiation [42]. Moreover, Nicolas et al. suggested that increased albumin may serve as a biomarker for UV-induced pathological change after observing greater levels of albumin in the retinas of monkeys with early onset macular degeneration than healthy monkeys [53].

The UVA dosages investigated in this study have physiological relevance in terms of both sun exposure and ophthalmological clinical treatment. After investigating the lethal dose of UVA radiation, we used doses of 5 and 10 J/cm² for the experiments conducted in this study. At peak sunlight between noon and 1:15 p.m. at a latitude of 11 degrees north of the equator, the UVA radiation has been measured to be as high as 6.59 mJ/cm² [54]. Thus, an exposure of only 12.6 min under these conditions would cumulatively equate to the lower (5 J/cm²) exposure used in this study. It is also possible that lesser exposures may accumulate and affect vision over time. While there is scant evidence for the dosimetric impact of radiation, several studies have found cumulative dose to be associated with visual acuity and blindness [55], as well as ocular structure and treatment toxicity [56].

Another condition in which humans may be exposed to UVA is through iatrogenic Means. UVA is now utilized clinically in the form of cross-linking (CXL). Combined UVA-riboflavin CXL has been increasingly used in the treatment of primary and secondary ectasia, such as keratoconus. One study used a total cumulative dose of 7.2 J/cm² UVA irradiation per eye over an 8 min duration [57]. However, this procedure raises concerns regarding the potential hazards of UVA to the anterior segment, and especially to the retina which is more sensitive to UVA light than light of other wavelengths [58, 59]. A prospective three-year study showed that corneal collagen CXL induced no iatrogenic macular toxicity as per optical coherence tomography [60]. However, a more recent study disclosed that most of the patients who had been continuously exposed to UVA

light during CXL therapy experienced slight changes in central macular thickness and multifocal electroretinography parameters [61]. Light toxicity may begin early following exposure but remain undetectable [62]. Thus, more frequent evaluations over shorter intervals following UVA-riboflavin CXL are recommended.

Conclusion

Our results indicate that proteomic analysis is a feasible method to explore and discover potential markers in ophthalmic disease and advance our understanding of the potent effects of UVA irradiation on ARPE-19 cells at the molecular level. The present study showed that UVA irradiation can significantly inhibit the proliferation of ARPE-19 cells. The unfolded protein stress caused by up-regulation of GRP-78 or downstream cascade proteins and mitochondrial dysfunction, cytochrome C release, and caspase-9 and caspase-3 activation all encourage cellular apoptosis. The results in our current study have not been reported yet. These findings are promising and warrant further study for the development of new therapeutic strategies against UVA exposure.

Acknowledgements

This study was supported by grants from Kaohsiung Medical University Hospital KMU97-7G04 and Yuan General Hospital RG12-002 for Hsien-Chung Lin and from National Science Council NSC 102-2313-B-276-002-MY3 for Yu-Jen Wu.

Authors' contributions

Conceived and designed the experiments: HCL and YJW. Performed the experiments: HCL and CTH. Analyzed the data: HCL and JLC. Wrote the paper: YJW, JLC, and JJK. All the authors have read and approved the manuscript.

Funding

This study was supported by grants from Kaohsiung Medical University Hospital KMU97-7G04 and Yuan General Hospital RG12-002 for Hsien-Chung Lin and from National Science Council NSC 102-2313-B-276-002-MY3 for Yu-Jen Wu.

Availability of data and materials

The data used in this study are provided in the figures and tables. The materials used in this study are cited in the text and are commercially available.

Ethics approval and consent to participate

Not applicable.

Consent for publication

Not applicable.

Competing interests

The authors declare that they have no competing interests.

Author details

¹Department of Ophthalmology, Kaohsiung Veterans General Hospital, Kaohsiung, Taiwan. ²School of Medicine, National Yang-Ming University, Taipei, Taiwan. ³Department of Optometry, Shu-Zen Junior College of Medicine and Management, Kaohsiung, Taiwan. ⁴Department of Ophthalmology, Yuan's General Hospital, Kaohsiung, Taiwan. ⁵College of Medicine, The Ohio State University, Columbus, OH, USA. ⁶School of Public Health, College of Public Health, Taipei Medical University, Taipei, Taiwan. ⁷International Master's Program, College of Health Technology, National

Taipei University of Nursing and Health Sciences, Taipei, Taiwan.

⁸Department of Ophthalmology, Kaohsiung Medical University Hospital, Kaohsiung, Taiwan. ⁹Department of Beauty Science, Meiho University, Pingtung, Taiwan.

Received: 28 July 2018 Accepted: 24 June 2019

Published online: 02 August 2019

References

- Wong WL, Su X, Li X, Cheung CM, Klein R, Cheng CY, Wong TY. Global prevalence and burden of age-related macular degeneration: a meta-analysis and disease burden projection for 2020 and 2040. *Lancet Glob Health*. 2014;2(2):e106–16. [https://doi.org/10.1016/S2214-109X\(13\)70145-1](https://doi.org/10.1016/S2214-109X(13)70145-1).
- Nowak JZ. Age-related macular degeneration (amd): pathogenesis and therapy. *Pharmacol Rep*. 2006;58(3):353–63.
- Winkler BS, Boulton ME, Gottsch JD, Sternberg P. Oxidative damage and age-related macular degeneration. *Mol Vis*. 1999;5:32.
- Cohen SY, Dubois L, Grenet T, Nghiem-Buffet S, Jung C, Fajnkuchen F, Delahaye-Mazza C, Quentel G, Tadayoni R. Peripapillary retinal pigment epithelium changes in age-related macular degeneration. *Retina*. 2016;36(3):458–64. <https://doi.org/10.1097/IAE.0000000000000741>.
- Hanus J, Anderson C, Wang S. Rpe necroptosis in response to oxidative stress and in amd. *Ageing Res Rev*. 2015;24(Pt B):286–98. <https://doi.org/10.1016/j.arr.2015.09.002>.
- Cai J, Nelson KC, Wu M, Sternberg P Jr, Jones DP. Oxidative damage and protection of the rpe. *Prog Retin Eye Res*. 2000;19(2):205–21. [https://doi.org/10.1016/S1350-9462\(99\)00009-9](https://doi.org/10.1016/S1350-9462(99)00009-9).
- Liang FQ, Godley BF. Oxidative stress-induced mitochondrial DNA damage in human retinal pigment epithelial cells: a possible mechanism for rpe aging and age-related macular degeneration. *Exp Eye Res*. 2003;76(4):397–403. [https://doi.org/10.1016/S0014-4835\(03\)00023-X](https://doi.org/10.1016/S0014-4835(03)00023-X).
- Plafker SM. Oxidative stress and the ubiquitin proteolytic system in age-related macular degeneration. *Adv Exp Med Biol*. 2010;664:447–56. https://doi.org/10.1007/978-1-4419-1399-9_51.
- Qin S. Oxidative damage of retinal pigment epithelial cells and age-related macular degeneration. *Drug Dev Res*. 2007;68(5):213–25. <https://doi.org/10.1002/ddr.20185>.
- Hollyfield JG, Bonilha VL, Rayborn ME, Yang X, Shadrach KG, Lu L, Ufret RL, Salomon RG, Perez VL. Oxidative damage-induced inflammation initiates age-related macular degeneration. *Nat Med*. 2008;14(2):194–8. <https://doi.org/10.1038/nm1709>.
- Chan CM, Huang JH, Lin HH, Chiang HS, Chen BH, Hong JY, Hung CF. Protective effects of (–)-epigallocatechin gallate on uva-induced damage in arpe19 cells. *Mol Vis*. 2008;14:2528–34.
- Evans JB, Syed BA. New hope for dry amd? *Nat Rev Drug Discov*. 2013;12(7):501–2. <https://doi.org/10.1038/nrd4038>.
- Johnson EJ. Age-related macular degeneration and antioxidant vitamins: recent findings. *Curr Opin Clin Nutr Metab Care*. 2010;13(1):28–33. <https://doi.org/10.1097/MCO.0b013e3283308ff>.
- Ma W, Zhao L, Fontainhas AM, Fariss RN, Wong WT. Microglia in the mouse retina alter the structure and function of retinal pigmented epithelial cells: a potential cellular interaction relevant to amd. *PLoS One*. 2009;4(11):e7945. <https://doi.org/10.1371/journal.pone.0007945>.
- Wielgus AR, Collier RJ, Martin E, Lih FB, Tomer KB, Chignell CF, Roberts JE. Blue light induced a2e oxidation in rat eyes—experimental animal model of dry amd. *Photochem Photobiol Sci*. 2010;9(11):1505–12. <https://doi.org/10.1039/c0pp00133c>.
- McCarty CA, Taylor HR. Recent developments in vision research: light damage in cataract. *Invest Ophthalmol Vis Sci*. 1996;37(9):1720–3.
- Glickman RD. Ultraviolet phototoxicity to the retina. *Eye Contact Lens*. 2011;37(4):196–205. <https://doi.org/10.1097/ICL.0b013e31821e45a9>.
- Kerr JB, McElroy CT. Evidence for large upward trends of ultraviolet-b radiation linked to ozone depletion. *Science*. 1993;262(5136):1032–4. <https://doi.org/10.1126/science.262.5136.1032>.
- Chalam KV, Khetpal V, Rusovici R, Balaiya S. A review: role of ultraviolet radiation in age-related macular degeneration. *Eye Contact Lens*. 2011;37(4):225–32. <https://doi.org/10.1097/ICL.0b013e31821fbd3e>.
- Patton WP, Chakravarthy U, Davies RJ, Archer DB. Comet assay of uv-induced DNA damage in retinal pigment epithelial cells. *Invest Ophthalmol Vis Sci*. 1999;40(13):3268–75.
- Roduit R, Schorderet DF. Map kinase pathways in uv-induced apoptosis of retinal pigment epithelium arpe19 cells. *Apoptosis*. 2008;13(3):343–53. <https://doi.org/10.1007/s10495-008-0179-8>.
- Tratsk KS, Thanos S. Uv irradiation causes multiple cellular changes in cultured human retinal pigment epithelium cells. *Graefes Arch Clin Exp Ophthalmol*. 2003;241(10):852–9. <https://doi.org/10.1007/s00417-003-0747-0>.
- McCubrey JA, Lahair MM, Franklin RA. Reactive oxygen species-induced activation of the map kinase signaling pathways. *Antioxid Redox Signal*. 2006;8(9–10):1775–89. <https://doi.org/10.1089/ars.2006.8.1775>.
- Sheu SJ, Wu SN. Mechanism of inhibitory actions of oxidizing agents on calcium-activated potassium current in cultured pigment epithelial cells of the human retina. *Invest Ophthalmol Vis Sci*. 2003;44(3):1237–44. <https://doi.org/10.1167/iovs.02-0330>.
- Roberts JE. Ocular phototoxicity. *J Photochem Photobiol B*. 2001;64(2–3):136–43. [https://doi.org/10.1016/S1011-1344\(01\)00196-8](https://doi.org/10.1016/S1011-1344(01)00196-8).
- Shaban H, Richter C. A2e and blue light in the retina: the paradigm of age-related macular degeneration. *Biol Chem*. 2002;383(3–4):537–45. <https://doi.org/10.1515/BC.2002.054>.
- Taylor HR, West S, Munoz B, Rosenthal FS, Bressler SB, Bressler NM. The long-term effects of visible light on the eye. *Arch Ophthalmol*. 1992;110(1):99–104.
- Delcourt C, Cougnard-Gregoire A, Boniol M, Carriere I, Dore JF, Delyfer MN, Rougier MB, Le Goff M, Dartigues JF, Barberger-Gateau P, et al. Lifetime exposure to ambient ultraviolet radiation and the risk for cataract extraction and age-related macular degeneration: the alienor study. *Invest Ophthalmol Vis Sci*. 2014;55(11):7619–27. <https://doi.org/10.1167/iovs.14-14471>.
- Neoh CA, Wang RY, Din ZH, Su JH, Chen YK, Tsai FJ, Weng SH, Wu YJ. Induction of apoptosis by sinulariolide from soft coral through mitochondrial-related and p38mapk pathways on human bladder carcinoma cells. *Mar Drugs*. 2012;10(12):2893–911. <https://doi.org/10.3390/md10122893>.
- Su CC, Chen JY, Din ZH, Su JH, Yang ZY, Chen YJ, Wang RY, Wu YJ. 13-acetoxysarcocrossolide induces apoptosis on human gastric carcinoma cells through mitochondria-related apoptotic pathways: P38/jnk activation and pi3k/akt suppression. *Mar Drugs*. 2014;12(10):5295–315. <https://doi.org/10.3390/md12105295>.
- Liu CI, Wang RY, Lin JJ, Su JH, Chiu CC, Chen JC, Chen JY, Wu YJ. Proteomic profiling of the 11-dehydrosinulariolide-treated oral carcinoma cells ca9-22: effects on the cell apoptosis through mitochondrial-related and er stress pathway. *J Proteome*. 2012;75(18):5578–89. <https://doi.org/10.1016/j.jprot.2012.07.037>.
- Li HH, Su JH, Chiu CC, Lin JJ, Yang ZY, Hwang WI, Chen YK, Lo YH, Wu YJ. Proteomic investigation of the sinulariolide-treated melanoma cells a375: effects on the cell apoptosis through mitochondrial-related pathway and activation of caspase cascade. *Mar Drugs*. 2013;11(7):2625–42. <https://doi.org/10.3390/md11072625>.
- Chen YJ, Su JH, Tsao CY, Hung CT, Chao HH, Lin JJ, Liao MH, Yang ZY, Huang HH, Tsai FJ, et al. Sinulariolide induced hepatocellular carcinoma apoptosis through activation of mitochondrial-related apoptotic and perk/eif2alpha/atf4/chop pathway. *Molecules*. 2013;18(9):10146–61. <https://doi.org/10.3390/molecules180910146>.
- Gehrs KM, Anderson DH, Johnson LV, Hageman GS. Age-related macular degeneration—emerging pathogenetic and therapeutic concepts. *Ann Med*. 2006;38(7):450–71. <https://doi.org/10.1080/07853890600946724>.
- Gonzalez-Girones DM, Moncunill-Massaguer C, Iglesias-Serret D, Cosiáls AM, Perez-Perarnau A, Palmeri CM, Rubio-Patino C, Villunger A, Pons G, Gil J. Aicar induces bax/bak-dependent apoptosis through upregulation of the bh3-only proteins bim and noxa in mouse embryonic fibroblasts. *Apoptosis*. 2013;18(8):1008–16. <https://doi.org/10.1007/s10495-013-0850-6>.
- Jiang X, Kanda T, Nakamoto S, Haga Y, Sasaki R, Nakamura M, Wu S, Mikata R, Yokosuka O. Knockdown of glucose-regulated protein 78 enhances poly(adp-ribose) polymerase cleavage in human pancreatic cancer cells exposed to endoplasmic reticulum stress. *Oncol Rep*. 2014;32(6):2343–8. <https://doi.org/10.3892/or.2014.3533>.
- Matsuo K, Gray MJ, Yang DY, Srivastava SA, Tripathi PB, Sonoda LA, Yoo EJ, Dubeau L, Lee AS, Lin YG. The endoplasmic reticulum stress marker, glucose-regulated protein-78 (grp78) in visceral adipocytes predicts endometrial cancer progression and patient survival. *Gynecol Oncol*. 2013;128(3):552–9. <https://doi.org/10.1016/j.ygyno.2012.11.024>.
- Winnay JN, Kahn CR. Pi 3-kinase regulatory subunits as regulators of the unfolded protein response. *Methods Enzymol*. 2011;490:147–58. <https://doi.org/10.1016/B978-0-12-385114-7.00009-X>.

39. Luo S, Baumeister P, Yang S, Abcouwer SF, Lee AS. Induction of grp78/bip by translational block: activation of the grp78 promoter by atf4 through and upstream atf/cre site independent of the endoplasmic reticulum stress elements. *J Biol Chem*. 2003;278(39):37375–85. <https://doi.org/10.1074/jbc.M303619200>.
40. Fernandez PM, Tabbara SO, Jacobs LK, Manning FC, Tsangaris TN, Schwartz AM, Kennedy KA, Patierno SR. Overexpression of the glucose-regulated stress gene grp78 in malignant but not benign human breast lesions. *Breast Cancer Res Treat*. 2000;59(1):15–26. <https://doi.org/10.1023/A:1006332011207>.
41. Rao RV, Peel A, Logvinova A, del Rio G, Hermel E, Yokota T, Goldsmith PC, Ellerby LM, Ellerby HM, Bredesen DE. Coupling endoplasmic reticulum stress to the cell death program: role of the er chaperone grp78. *FEBS Lett*. 2002; 514(2–3):122–8. [https://doi.org/10.1016/S0014-5793\(02\)02289-5](https://doi.org/10.1016/S0014-5793(02)02289-5).
42. Kraljevic Pavelic S, Klobucar M, Sedick M, Micek V, Gehrig P, Grossman J, Pavelic K, Vojnikovic B. Uv-induced retinal proteome changes in the rat model of age-related macular degeneration. *Biochim Biophys Acta*. 2015; 1852(9):1833–45. <https://doi.org/10.1016/j.bbdis.2015.06.006>.
43. Moran SD, Zhang TO, Decatur SM, Zanni MT. Amyloid fiber formation in human gammaD-crystallin induced by uv-b photodamage. *Biochemistry*. 2013;52(36):6169–81. <https://doi.org/10.1021/bi4008353>.
44. Xia Z, Yang Z, Huynh T, King JA, Zhou R. Uv-radiation induced disruption of dry-cavities in human gammaD-crystallin results in decreased stability and faster unfolding. *Sci Rep*. 2013;3:1560. <https://doi.org/10.1038/srep01560>.
45. Piatigorsky J. Lens crystallins and their genes: diversity and tissue-specific expression. *FASEB J*. 1989;3(8):1933–40.
46. Sreekumar PG, Kannan R, Kitamura M, Spee C, Barron E, Ryan SJ, Hinton DR. Alphas crystallin is apically secreted within exosomes by polarized human retinal pigment epithelium and provides neuroprotection to adjacent cells. *PLoS One*. 2010;5(10):e12578. <https://doi.org/10.1371/journal.pone.0012578>.
47. Zhou P, Kannan R, Spee C, Sreekumar PG, Dou G, Hinton DR. Protection of retina by alphaB crystallin in sodium iodate induced retinal degeneration. *PLoS One*. 2014;9(5):e98275. <https://doi.org/10.1371/journal.pone.0098275>.
48. Yu DY, Cringle SJ. Oxygen distribution and consumption within the retina in vascularised and avascular retinas and in animal models of retinal disease. *Prog Retin Eye Res*. 2001;20(2):175–208. [https://doi.org/10.1016/S1350-9462\(00\)00027-6](https://doi.org/10.1016/S1350-9462(00)00027-6).
49. Yokosako K, Mimura T, Funatsu H, Noma H, Goto M, Kamei Y, Kondo A, Matsubara M. Glycolysis in patients with age-related macular degeneration. *Open Ophthalmol J*. 2014;8:39–47. <https://doi.org/10.2174/1874364101408010039>.
50. Zuniga FI, Craft CM. Deciphering the structure and function of als2c4r in the mouse retina. *Invest Ophthalmol Vis Sci*. 2010;51(9):4407–15. <https://doi.org/10.1167/iovs.10-5251>.
51. Narimatsu T, Ozawa Y, Miyake S, Kubota S, Hirasawa M, Nagai N, Shimmura S, Tsubota K. Disruption of cell-cell junctions and induction of pathological cytokines in the retinal pigment epithelium of light-exposed mice. *Invest Ophthalmol Vis Sci*. 2013;54(7):4555–62. <https://doi.org/10.1167/iovs.12-11572>.
52. Cachafeiro M, Bemelmans AP, Samardzija M, Afanasieva T, Pournaras JA, Grimm C, Kostic C, Philippe S, Wenzel A, Arsenijevic Y. Hyperactivation of retina by light in mice leads to photoreceptor cell death mediated by vegf and retinal pigment epithelium permeability. *Cell Death Dis*. 2013;4:e781. <https://doi.org/10.1038/cddis.2013.303>.
53. Nicolas MG, Fujiki K, Murayama K, Suzuki MT, Mineki R, Hayakawa M, Yoshikawa Y, Cho F, Kanai A. Studies on the mechanism of early onset macular degeneration in cynomolgus (macaca fascicularis) monkeys. I. Abnormal concentrations of two proteins in the retina. *Exp Eye Res*. 1996; 62(3):211–9. <https://doi.org/10.1006/exer.1996.0026>.
54. Balasaraswathy P, Kumar U, Srinivas CR, Nair S. UVA and UVB in sunlight, optimal utilization of UV rays in sunlight for phototherapy. *Indian J Dermatol Venereol Leprol*. 2002;68(4):198–201.
55. Jensen AW, Petersen IA, Kline RW, Stafford SL, Schomberg PJ, Robertson DM. Radiation complications and tumor control after 125I plaque brachytherapy for ocular melanoma. *Int J Radiat Oncol Biol Phys*. 2005;63(1):101–8.
56. Wagner A, Chen A, Cook T, Faber D, Winward K, Sause W. Outcomes and control rates for I-125 plaque brachytherapy for uveal melanoma: a community-based institutional experience. *ISRN Ophthalmol*. 2014;2014: 950975. <https://doi.org/10.1155/2014/950975>.
57. Jiang LZ, Jiang W, Qiu SY. Conventional vs. pulsed-light accelerated corneal collagen cross-linking for the treatment of progressive keratoconus: 12-month results from a prospective study. *Exp Ther Med*. 2017;14(5):4238–44.
58. Goldich Y, Marcovich AL, Barkana Y, Avni I, Zadok D. Safety of corneal collagen cross-linking with UV-A and riboflavin in progressive keratoconus. *Cornea*. 2010;29(4):409–11.
59. Ham WT, Mueller HA, Sliney DH. Retinal sensitivity to damage from short wavelength light. *Nature*. 1976;260:153–5.
60. Poli M, Cornut PL, Balmitgere T, Aptel F, Janin H, Burillon C. Prospective study of corneal collagen cross-linking efficacy and tolerance in the treatment of keratoconus and corneal ectasia: 3-year results. *Cornea*. 2013;32:583–90.
61. Barbisan PRT, Vitorino MGM, Souto FMS, Tian B, Pacheco Pinto RD, Quagliato LB, Nascimento MA, de Castro RS, Arieta CEL. Macular phototoxicity after corneal cross-linking. *Clin Ophthalmol*. 2018;12:1801–7.
62. Mirzaei M, Bagheri M, Taher A. Influence of standard corneal cross-linking in keratoconus patients on macular profile. *J Curr Ophthalmol*. 2018;30:330–6.

Publisher's Note

Springer Nature remains neutral with regard to jurisdictional claims in published maps and institutional affiliations.

Ready to submit your research? Choose BMC and benefit from:

- fast, convenient online submission
- thorough peer review by experienced researchers in your field
- rapid publication on acceptance
- support for research data, including large and complex data types
- gold Open Access which fosters wider collaboration and increased citations
- maximum visibility for your research: over 100M website views per year

At BMC, research is always in progress.

Learn more biomedcentral.com/submissions

